

Concept-Level Explanation for the Generalization of a DNN

Huilin Zhou¹ Hao Zhang¹ Huiqi Deng¹ Dongrui Liu¹
Wen Shen¹ Shih-Han Chan² Quanshi Zhang^{1*}

¹Shanghai Jiao Tong University

²University of California San Diego

Abstract

This paper explains the generalization power of a deep neural network (DNN) from the perspective of interactive concepts. Many recent studies [Deng et al. \[2021a\]](#), [Ren et al. \[2022, 2021\]](#) have quantified a clear emergence of interactive concepts encoded by the DNN, which have been observed on different DNNs during the learning process. Therefore, in this paper, we investigate the generalization power of each interactive concept, and we use the generalization power of different interactive concepts to explain the generalization power of the entire DNN. Specifically, we define the complexity of each interactive concept. We find that simple concepts can be better generalized to testing data than complex concepts. The DNN with strong generalization power usually learns simple concepts more quickly and encodes fewer complex concepts. More crucially, we discover the detouring dynamics of learning complex concepts, which explain both the high learning difficulty and the low generalization power of complex concepts.

1. Introduction

Although deep neural networks (DNNs) have achieved remarkable success in various tasks in recent years, the essential reason for the significant generalization power of a DNN is still unclear. People usually explained DNNs from different perspectives, *e.g.*, examining the flatness of the loss landscape [Keskar et al. \[2016\]](#), deriving the theoretical bounds for the generalization [Dziugaite and Roy \[2017b\]](#), [Neyshabur et al. \[2015\]](#), and developing some metrics for the representation power [Fort et al. \[2019\]](#), [Weng et al. \[2018\]](#).

Unlike the above studies, in this paper, we revisit the generalization power of a DNN from a new perspective, *i.e.*, the generalization power may be owing to the fact that the DNN encodes generalizable concepts for inference.

*Quanshi Zhang is the corresponding author. He is with the Department of Computer Science and Engineering, the John Hopcroft Center, at the Shanghai Jiao Tong University, China. <zqs1022@sjtu.edu.cn>

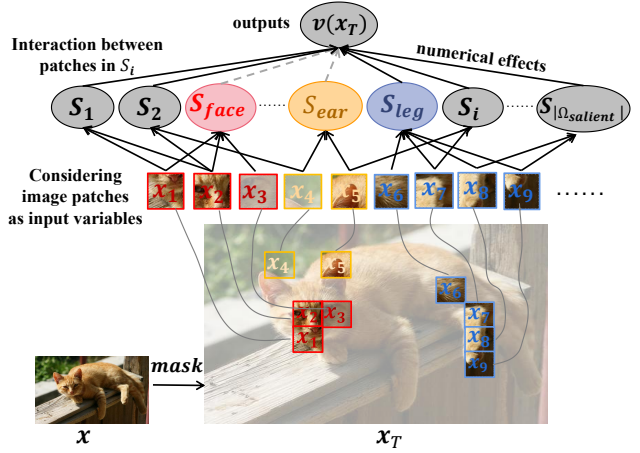


Figure 1. Explaining network inferences using interactive concepts. Given an input sample x with n input variables, we can get 2^n different samples when some input variables are randomly masked. We can usually use numerical effects of only tens of concepts to well fit the network outputs on all 2^n masked samples x_T .

Concept-emergence phenomenon. Unlike graphical models, a DNN does not provide physical units to explicitly encode certain symbolic concepts. In spite of that, the emergence of visual concepts has been observed by [Ren et al. \[2021\]](#) on different DNNs trained for various tasks. Specifically, the DNN usually does not use each input variable (*e.g.*, a pixel in an image or a word in a sentence) for inference independently. Instead, the DNN usually encodes various interactions between different input variables for inference. [Ren et al. \[2021, 2022\]](#), [Deng et al. \[2021a\]](#) have found that a few interactions directly make numerical effects on the inference score of the DNN. Furthermore, [Ren et al. \[2022\]](#) used such interactive concepts to derive the optimal baseline value of input variables. [Deng et al. \[2021a\]](#) proved the representation bottleneck of the DNN based on such interactive concepts.

Therefore, each interaction with considerable effects on the inference score can be considered as a specific *interactive concept*, which represents an AND relationship between a

set of input variables encoded by the DNN. For example, in Figure 1, the face concept consists of patches of the $S = \{\text{eyes, nose, mouth}\}$, which represents an AND relationship between all these three patches $x_i (i \in S)$. Only if all patches in the concept S are present, the concept S is activated and makes a numerical effect on the network output. The masking of any patches will deactivate this concept S and remove the effect.

More crucially, given an input sample x with n input variables, we have 2^n ways to mask the input sample. Ren et al. [2021] have proven that the network outputs of all the 2^n different masked samples could be well mimicked by the numerical effects of a few interactive concepts. This guarantees the faithfulness of considering such interactive concepts as inference patterns encoded by the DNN.

Explaining generalization power using interactive concepts. Unlike previous studies, the emergence of interactive concepts provides us a more straightforward way to analyze the representation power of a DNN, *i.e.*, people can directly examine whether the DNN learns generalizable concepts for inference. **Let a concept be frequently extracted by the DNN from training samples. If this concept is generalizable, then this concept is supposed to also frequently appear in testing samples. Otherwise, the concept is considered to have poor generalization power.** Compared to previous studies, we believe that such an examination of the disentangled concepts is *a more straightforward way to analyze the generalization power of a DNN.*

Building up connections between the complexity of interactive concepts and the generalization power. The core of this study is to explore the relationship between interactive concepts and their generalization power. Although it is impractical to visualize each concept manually and then one-by-one check which concept frequently appears in testing samples, in this study, *we still discover and theoretically explain the strong tendency that complex concepts are usually over-fitted.* Specifically, if an interactive concept S contains many input variables, then we consider it to be a complex concept, and the number of input variables is termed the *order* of the concept, *i.e.*, $\text{order}(S) = |S|$. In this way, a low-order interactive concept represents a simple pattern consisting of a few input variables.

We discover that concepts of low orders usually have stronger generalization power than concepts of high orders. Specifically, we investigate the generalization power from the following four perspectives.

- For each concept, we compute the distribution of its effects on training samples and such a distribution on testing samples. We find that compared to the distribution of high-order concepts, the distribution of low-order concepts in training samples and that in testing samples are usually more similar to each other. This indicates strong generalization power of low-order concepts.

- Let us focus on a set of DNNs with the same architecture, which are managed to be trained at different over-fitting levels. We find that over-fitted DNNs usually encode stronger high-order interactive concepts than normal DNNs.

- Besides, normal DNNs usually learn low-order interactive concepts more quickly than over-fitted DNNs.

- Categories, whose inferences are sensitive to small perturbations on the input, usually encode stronger high-order concepts than categories that are robust to perturbations.

In fact, all above phenomena can be partially explained by the following two observations. First, both the low generalization power and the slow learning speed of high-order concepts can also be explained by the detouring dynamics of learning high-order concepts. Specifically, we find that a high-order concept is more likely to be mistakenly represented by the DNN as a mixture of low-order concepts. In comparison, a low-order concept is more likely to be learned directly. This indicates that high-order concepts are more difficult to be learned correctly.

Second, both the low generalization power and the high noise sensitivity of high-order interactions are also related to the increasing variance of concepts' effects along with the order.

2. Explaining generalization using concepts

2.1. Preliminaries: sparse interactive concepts

The layer-wise processing of features in a DNN seems to conflict with the symbolic representation of concepts. However, many recent studies Deng et al. [2021a], Ren et al. [2021, 2022] have observed the phenomenon of concept emergence on different DNNs trained for various tasks. Specifically, given a sufficiently-trained DNN v for classification and an input sample $x = [x_1, x_2, \dots, x_n]^T$ with n input variables, let $N = \{1, 2, \dots, n\}$ denote the indices of all n input variables in x , and let $v(x) \in \mathbb{R}$ denote the scalar output of the DNN or a certain output dimension of the DNN¹. Then, Ren et al. [2021] have defined each concept memorized by a DNN to represent the interaction between a set $S \subseteq N$ of input variables, which has been encoded by the DNN. More crucially, it proves that the inference score $v(x)$ on the sample x can be mathematically disentangled into numerical effects of different interactions,

$$v(x) = \sum_{S \subseteq N} I(S|x) \quad (1)$$

where $I(S|x)$ quantifies the numerical effect of the interaction between input variables in the subset $S \subseteq N$.

Defining salient interactions as concepts. It is found that only a relatively small number of interactions have non-

¹Note that people can apply different settings for $v(x)$. In particular, for multi-category classification tasks, we set $v(x) = \log \frac{p(y=y_{\text{truth}}|x)}{1-p(y=y_{\text{truth}}|x)} \in \mathbb{R}$ by following Deng et al. [2021a].

ignorable effects $|I(S|\mathbf{x})|$. Thus, each salient interaction S between variables in S can be considered as a *concept* encoded by the DNN with significant influence on the network output. In comparison, most interactions have almost zero effect, *i.e.*, $I(S|\mathbf{x}) \approx 0$, and we do not consider such interactions as valid concepts.

The numerical effect $I(S|\mathbf{x})$ between input variables in each subset $S \subseteq N$ is measured as the Harsanyi dividend [Harsanyi \[1982\]](#), *i.e.*, $\forall S \subseteq N, I(S|\mathbf{x}) = \sum_{T \subseteq S} (-1)^{|S|-|T|} \cdot v(\mathbf{x}_T)$. Here, \mathbf{x}_T represents a masked sample, where input variables in $N \setminus T$ are masked with their baseline values².

Understanding interactive concepts. Each interactive concept, *i.e.*, an interaction with considerable effect $I(S|\mathbf{x})$, can be considered to represent the AND relationship between input variables in S . For example, in Figure 1, the face concept consists of all image patches in the set $S_{\text{face}} = \{x_1 = \text{eyes}, x_2 = \text{mouth}, x_3 = \text{nose}\}$. Only when all the three image patches in S_{face} are present in the input sample \mathbf{x} , the face concept S_{face} is activated and makes a numerical effect $I(S_{\text{face}}|\mathbf{x})$ on the network output. If any image patch in S_{face} is absent (or masked), then the face concept S_{face} is deactivated, *i.e.*, making $I(S_{\text{face}}|\mathbf{x}) = 0$.

Sparsity and universal approximation ensure the faithfulness of concepts. Does a DNN really encode concepts? Why is the so-called interactive concept measured by $I(S|\mathbf{x})$ a faithful measurement of the concept? These are two core questions for the concept-emerging phenomenon beyond the mathematical formulations of Equation (1) and the Harsanyi dividend.

According to Occam’s Razor [Blumer et al. \[1987\]](#), if the inference score can be explained as just a few concepts, rather than a huge number of concepts, then the concept is more likely to reflect the true concepts encoded by a DNN, instead of a mathematical trick that satisfies Equation (1). [Ren et al. \[2021, 2022\]](#), [Deng et al. \[2021a\]](#) have found that given each of the various DNNs trained for different tasks, its inference score is usually explained as sparse interactive concepts. As Figure 2 (a) shows, $I(S|\mathbf{x})$ of most interactive concepts are almost zero, and only a few salient concepts in Ω_{salient} influence the output score. More importantly, it is proven that such **sparse salient concepts** can **universally approximate** network outputs of all 2^n different randomly masked samples $\forall T \subseteq N, \mathbf{x}_T$,

$$\forall T \subseteq N, v(\mathbf{x}_T) = \sum_{S \subseteq T: S \in \Omega_{\text{salient}}} I(S|\mathbf{x}) + \epsilon_T \quad (2)$$

where the residual term $\epsilon_T = \sum_{S \subseteq T: S \notin \Omega_{\text{salient}}} I(S|\mathbf{x})$ represents the sum of interactive effects of all non-salient interactive concepts. For most DNNs, people can use only a

²The baseline value of each input variable is usually implemented as the mean value of this input variable over all samples [Dabkowski and Gal \[2017\]](#).

small number of interactive concepts (empirically 10-100 interactive concepts) to approximately explain $v(\mathbf{x}_T)$ and leave a relatively small residual term ϵ_T .

2.2. High-order concepts are more over-fitted

In the previous subsection, we have introduced that given an input sample and a well-trained DNN, the inference score on all randomly masked samples can be universally synthesized by sparse interactive concepts. Then, in this subsection, let us investigate how to explain the over-fitting level of the DNN from the perspective of interactive concepts.

Specifically, we find that *complex interactive concepts are usually more over-fitted than relatively simple interactive concepts*. Here, we use the number of input variables in the interactive concept S to measure the complexity of the concept, which is also termed the **order** of the concept, *i.e.*, $\text{order}(S) = |S|$. A low-order interactive concept represents the interaction between a small number of input variables, which is usually considered to be a simple concept. A high-order interactive concept represents the complex interaction between a large number of input variables.

We have conducted various experiments to verify that encoding of complex concepts makes a DNN more over-fitted. We then try to use the concept’s stability to partially explain our findings.

2.2.1 Illustrating concepts of different orders

Before investigating the relationship between the complexity of concepts and the generalization power of a DNN, let us first visualize interactive concepts extracted from a DNN. Specifically, we trained a seven-layer MLP network (MLP-7-census) on the census dataset [Asuncion and Newman \[2007\]](#) and a seven-layer MLP network (MLP-7-TV) on the TV news dataset [Asuncion and Newman \[2007\]](#), respectively. Each layer of the MLPs contained 100 neurons. We also trained AlexNet [Krizhevsky et al. \[2017\]](#), ResNet-20 [He et al. \[2016\]](#), and VGG-11 [Simonyan and Zisserman \[2014\]](#) on the MNIST dataset [LeCun et al. \[1998\]](#) (AlexNet-MNIST, ResNet-20-MNIST, VGG-11-MNIST) and the CIFAR-10 dataset [Krizhevsky et al. \[2009\]](#) (AlexNet-CIFAR-10, ResNet-20-CIFAR-10, VGG-11-CIFAR-10).

Given each DNN and an input sample $\mathbf{x} \in \mathbb{R}^n$, we computed numerical effects $I(S|\mathbf{x})$ of all 2^n potential interactions, $S \subseteq N$. We found a common phenomenon that interactive concepts encoded by a DNN were usually very **sparse**, which ubiquitously existed in different DNNs. As Figure 2 (a) shows, numerical effects of 80%-95% interactive concepts were almost zero ($|I(S|\mathbf{x})| \approx 0$), and only a few salient interactive concepts had relatively significant effects $|I(S|\mathbf{x})|$. This finding was also consistent with the conclusion found by [Ren et al. \[2021, 2022\]](#), [Deng et al. \[2021a\]](#). The sparsity of interactive concepts ensured the

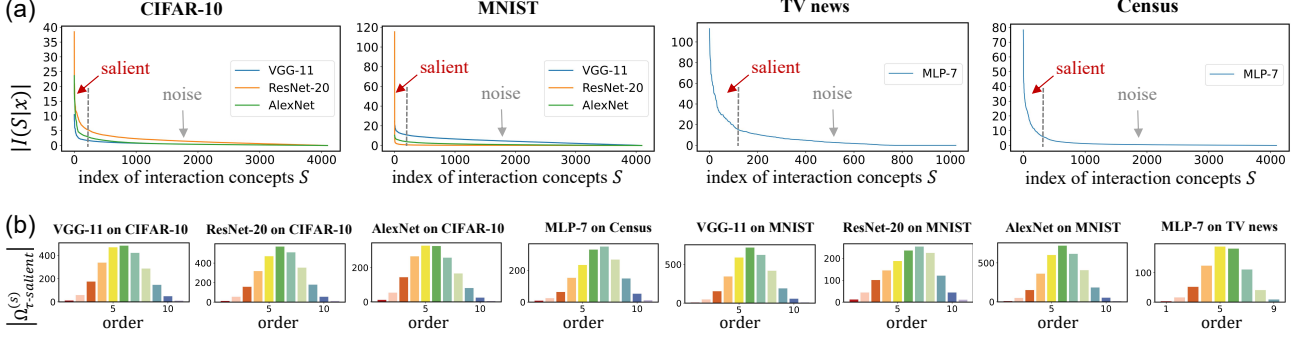


Figure 2. (a) Interactive concepts encoded by a DNN are usually very sparse. This phenomenon exists in various DNNs trained on different datasets. We sort the interactive concepts to a decreasing order of the interaction strength $|I(S|\mathbf{x})|$. (b) Histogram of salient concepts of different orders, $|\Omega_{\tau\text{-salient}}^{(s)}|$.

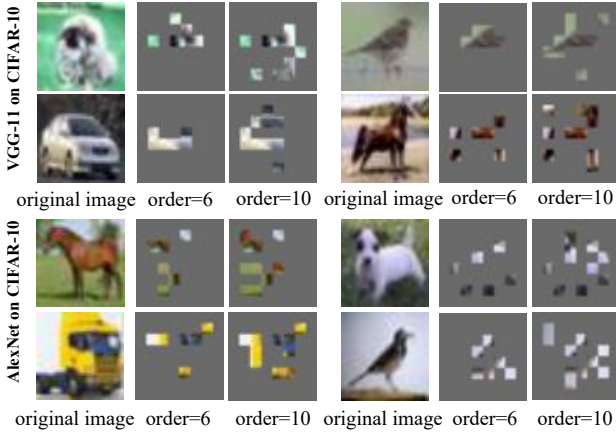


Figure 3. Visualization of salient concepts of different orders. Each salient interaction between the visualized patches contributes a considerable numerical effect to the inference score.

trustworthiness of such a concept definition.

Moreover, for each DNN, we compared the number of salient concepts of different complexities. Given a threshold τ , we defined the set of salient concepts $\Omega_{\tau\text{-salient}}$ as interactive concepts whose strength was greater than the threshold τ , *i.e.*, $\Omega_{\tau\text{-salient}} = \{S : |I(S|\mathbf{x})| > \tau\}$. Accordingly, $\Omega_{\tau\text{-salient}}^{(s)} = \{S : |I(S|\mathbf{x})| > \tau \text{ and } |S| = s\}$ represented all salient concepts of the s -th order. Figure 2 (b) shows the number of salient concepts of different orders, $|\Omega_{\tau\text{-salient}}^{(s)}|$, where the threshold was set to be $\tau = 0.05 \cdot \max_S |I(S|\mathbf{x})|$. This figure illustrates that there were more middle-order salient concepts than low-order salient concepts and high-order salient concepts.

Finally, in Figure 3, we visualized several representative salient concepts, covering low-order, middle-order, and high-order concepts. We used the aforementioned AlexNet-CIFAR-10 and VGG-11-CIFAR-10, and we set the threshold $\tau = 0.05 \cdot \max_S |I(S|\mathbf{x})|$. We found that salient concepts of different orders were usually made up by the image patches that contained the discriminative parts of the object.

2.2.2 Generalization to testing samples

This subsection aims to verify that **compared to high-order interactive concepts, low-order interactive concepts are more likely to have the distribution in training samples being similar to the distribution in testing samples**. Compared to previous studies using the gap of the loss Dziugaite and Roy [2017b], Neyshabur et al. [2017], Bartlett et al. [2017], Bousquet et al. [2020], Deng et al. [2021b], Haghi-fam et al. [2020, 2021] or the smoothness of the loss landscape Keskar et al. [2016], Li et al. [2018], Foret et al. [2021], Kwon et al. [2021] to investigate the generalization power of a DNN, the disentanglement of interactive concepts provides us *a new and more straightforward perspective* to define the generalization power of a DNN. *I.e.*, *if an interactive concept is frequently extracted by the DNN from training samples, then it is also supposed to frequently appear in testing samples. Otherwise, the interactive concept is not considered to be well generalized.*

In this way, we can define the generalization power of m -order interactive concepts *w.r.t.* the category c as the similarity between the distribution of m -order interactive concepts in training samples of category c and that in testing samples of category c . Let the vector $I_{\text{train},c}^{(m)} = [I_{\text{train},c}^{(m)}(S_1), I_{\text{train},c}^{(m)}(S_2), \dots, I_{\text{train},c}^{(m)}(S_d)]^T \in \mathbb{R}^d$ represent the distribution of m -order interactive concepts over training samples in the category c , which enumerates all the $d = \binom{n}{m}$ possible m -order interactive concepts. The i -th dimension $I_{\text{train},c}^{(m)}(S_i) = \mathbb{E}_{\mathbf{x} \in D_{\text{train},c}} [I(S_i|\mathbf{x})]$ represents the average effect of the interactive concept S_i over different training samples in the category c . Accordingly, the vector $I_{\text{test},c}^{(m)}$ denotes the distribution of m -order concepts over testing samples in the category c . Then, the similarity of the concept distribution between training samples and testing samples is given as the Jaccard similarity between $\tilde{I}_{\text{train},c}^{(m)}$ and $\tilde{I}_{\text{test},c}^{(m)}$,

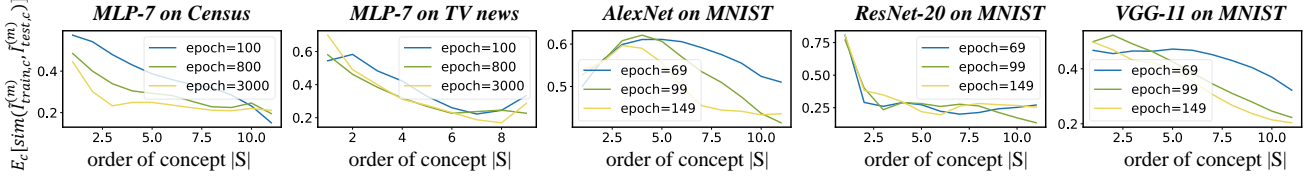


Figure 4. Average similarity between interactive concepts extracted from training images and those extracted from testing images.

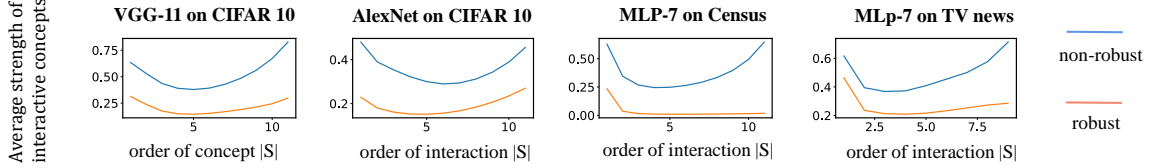


Figure 5. Average strength $\mathbb{E}_{c \in C_{\text{robust}}} \mathbb{E}_{\mathbf{x} \in D_c} \mathbb{E}_{S: |S|=m} [I^{(m)}(S|\mathbf{x})]$ of interactive concepts extracted from robust categories and the average strength $\mathbb{E}_{c \in C_{\text{non-robust}}} \mathbb{E}_{\mathbf{x} \in D_c} \mathbb{E}_{S: |S|=m} [I^{(m)}(S|\mathbf{x})]$ of interactive concepts extracted from non-robust categories.

$$\text{sim}(\tilde{I}_{\text{train},c}^{(m)}, \tilde{I}_{\text{test},c}^{(m)}) = \frac{\|\min(\tilde{I}_{\text{train},c}^{(m)}, \tilde{I}_{\text{test},c}^{(m)})\|_1}{\|\max(\tilde{I}_{\text{train},c}^{(m)}, \tilde{I}_{\text{test},c}^{(m)})\|_1} \quad (3)$$

where we extend the d -dimensional vector $I_{\text{train},c}^{(m)}$ into a $2d$ -dimensional vector $\tilde{I}_{\text{train},c}^{(m)} = [(I_{\text{train},c}^{(m),+})^T, (-I_{\text{train},c}^{(m),-})^T]^T = [(\max(I_{\text{train},c}^{(m)}, 0))^T, (-\min(I_{\text{train},c}^{(m)}, 0))^T]^T \in \mathbb{R}^{2d}$ with non-negative elements. Similarly, $\tilde{I}_{\text{test},c}^{(m)}$ is constructed on $I_{\text{test},c}^{(m)}$ to contain non-negative elements. Thus, a high similarity $\text{sim}(\tilde{I}_{\text{train},c}^{(m)}, \tilde{I}_{\text{test},c}^{(m)})$ indicates that most m -order interactive concepts in the category c can be well generalized to testing samples in the category c .

Furthermore, we conducted experiments to check whether high-order interactive concepts were more likely to be overfitted. Specifically, we trained a simple MLP with seven layers for tabular dataset, including the census dataset and the TV news dataset. We also trained AlexNet, VGG-11 and ResNet-20 on the MNIST dataset. Given each DNN, we computed interactive concepts of each order m . For each category c , we measured the above conceptual similarity for m -order interactive concepts, and Figure 4 reports the average similarity over different categories, *i.e.*, $\text{similarity} = \mathbb{E}_c[\text{sim}(\tilde{I}_{\text{train},c}^{(m)}, \tilde{I}_{\text{test},c}^{(m)})]$. We found that low-order interactive concepts usually had more similar distributions between training samples and testing samples than high-order interactive concepts. This meant that compared to high-order concepts, the DNN was more likely to extract similar low-order concepts from the training data and testing data. In other words, low-order concepts in training data could be better generalized to testing data.

2.2.3 Sensitiveness of high-order concepts

This subsection aims to verify the claim that **non-robust categories tend to encode stronger high-order interactive concepts**. Intuitively, features that are robust to inevitable

noises in data are usually more reliable and can be better generalized to testing samples, because small noises do not hurt the classification. Thus, inspired by this, we train a DNN, to make the classification of some categories sensitive to noises and make the classification of other categories robust to noises. This experiment is designed to examine whether non-robust categories activate more high-order interactive concepts than robust categories. If so, it can partially prove that high-order interactive concepts have poorer generalization power.

Therefore, in experiments, we trained different DNNs. For each DNN, the classification of some categories was adversarially trained, and the classification of other categories was normally trained. In this way, we could roughly consider that the feature representations of the adversarially trained categories were more robust to noises and could be better generalized to testing samples³, just like the previous findings Arpit et al. [2017].

We trained AlexNet and VGG-11 on the CIFAR-10 dataset Krizhevsky et al. [2009]. The first five categories in $C_{\text{non-robust}} = \{\text{airplane, automobile, bird, cat, deer}\}$ were normally trained, and the last five categories in $C_{\text{robust}} = \{\text{dog, frog, horse, ship, truck}\}$ were adversarially trained. We also trained five-layer MLPs on the *census* dataset and the *TV news* dataset. For each tabular dataset, we learned two seven-layer MLPs, one that was adversarially trained and one that was normally trained.

We computed the average interaction strength of interactive concepts of different orders over different training samples in the category c , *i.e.*, $\mathbb{E}_{\mathbf{x} \in D_c} \mathbb{E}_{S: |S|=m} [I^{(m)}(S|\mathbf{x})]$. Figure 5 compared the average interaction strength extracted from robust categories in C_{robust} with the average interaction strength extracted from non-robust categories in $C_{\text{non-robust}}$. It shows that non-robust categories activated stronger high-

³ Ilyas et al. [2019] considered adversarial training still removed some discriminative yet non-robust features from the DNN.

order interactive concepts than robust categories.

2.2.4 Proof of the sensitivity of concepts

All experimental findings in the above subsections is related to the phenomenon that high-order concepts are more sensitive to small noises in the input sample than low-order interactive concepts, thereby not being stably extracted. Therefore, in this subsection, we aim to prove that **the high-order interaction concept is usually more sensitive to input perturbations than the low-order interactive concept**. Let us add a Gaussian perturbation $\epsilon \sim \mathcal{N}(\mathbf{0}, \delta^2 \mathbf{I})$ to the input sample \mathbf{x} and obtain $\mathbf{x}' = \mathbf{x} + \epsilon$. Actually, noises/variations inevitably exist in the data, such as chaotic textures on an object or the scale/position change for an object during object detection, which are usually difficult to model. Therefore, we use the Gaussian perturbation to represent the noises/variations in the data for simplicity. Then, Theorem 2 reformulates the interactive effect $I(S|\mathbf{x}')$ using the Taylor series expansion.

Lemma 1. *Given a neural network v and an arbitrary perturbed input sample $\mathbf{x}' = \mathbf{x} + \epsilon$, the neural network output $v(\mathbf{x}')$ can be rewritten by following the Taylor series expansion at the baseline point $\mathbf{b} = [b_1, \dots, b_n]^T$,*

$$v(\mathbf{x}') = v(\mathbf{b}) + \sum_{k=1}^{\infty} \sum_{\kappa \in O_k} C(\kappa) \cdot \nabla_v(\kappa) \cdot \pi(\kappa|\mathbf{x}'), \quad (4)$$

including the coefficient $C(\kappa) = \frac{1}{(\kappa_1 + \dots + \kappa_n)!} \binom{\kappa_1 + \dots + \kappa_n}{\kappa_1, \dots, \kappa_n} \in \mathbb{R}$, the partial derivative $\nabla_v(\kappa) = \frac{\partial^{\kappa_1 + \dots + \kappa_n} v(\mathbf{b})}{\partial^{\kappa_1} x_1 \dots \partial^{\kappa_n} x_n} \in \mathbb{R}$, and the expansion term $\pi(\kappa|\mathbf{x}') = \prod_{i=1}^n (x'_i - b_i)^{\kappa_i}$. Here, $\kappa = [\kappa_1, \dots, \kappa_n] \in \mathbb{N}^n$ denotes the non-negative integer degree vector of each Taylor expansion term. Correspondingly, $O_k = \{\kappa \in \mathbb{N}^n | \kappa_1 + \dots + \kappa_n = k\}$ represents the set of all expansion terms of the k -th order.

Lemma 1 gives the Taylor series expansion when the network output $v(\mathbf{x}')$ is expanded at the baseline point $\mathbf{b} = [b_1, \dots, b_n]^T$. In this subsection, we use the baseline value b_i to represent the masking state of the input variable x_i . Normally, we can set the input variable x_i as the average value of x_i over different samples to remove the information Ancona et al. [2019], i.e., $b_i = \mu_i = \mathbb{E}_{\mathbf{x}}[x_i]$. However, pushing the input variable x_i a big distance $\tau \in \mathbb{R}$ towards μ_i is usually enough to remove the information in real applications. Therefore, we temporarily set $b_i = x_i + \tau$, if $x_i < \mu_i$; and set $b_i = x_i - \tau$, if $x_i > \mu_i$, in order to simplify the proof.

Theorem 2. *Given a neural network v and an arbitrary perturbed input sample $\mathbf{x}' = \mathbf{x} + \epsilon$ by adding a Gaussian perturbation $\epsilon \sim \mathcal{N}(\mathbf{0}, \delta^2 \mathbf{I})$, the interactive effect $I(S|\mathbf{x}')$ is defined by setting $(\mathbf{x}'_T)_i = x'_i$ if $i \in T$ and setting $(\mathbf{x}'_T)_i = b_i$*

if $i \notin T$. Then, we obtain

$$\begin{aligned} I(S|\mathbf{x}') &= \sum_{\kappa \in Q_S} C(\kappa) \cdot \nabla_v(\kappa) \cdot \pi(\kappa|\mathbf{x}') \\ &= \sum_{\kappa \in Q_S} Z(\kappa) \cdot \hat{\pi}(\kappa|\mathbf{x}') \end{aligned} \quad (5)$$

where $\hat{\pi}(\kappa|\mathbf{x}') = \prod_{i=1}^n \left(\frac{\text{sign}(x_i - b_i)}{\tau} \right)^{\kappa_i} \cdot \pi(\kappa|\mathbf{x}')$ is a standard AND interaction of the degree vector κ , and it is normalized to satisfy $\forall \kappa \in Q_S, \mathbb{E}_{\epsilon}[\hat{\pi}(\kappa|\mathbf{x}' = \mathbf{x} + \epsilon)] = 1 + O(\delta^2)$. In addition, $Z(\kappa) = \prod_{i=1}^n \left(\frac{\tau}{\text{sign}(x_i - b_i)} \right)^{\kappa_i} \cdot C(\kappa) \cdot \nabla_v(\kappa)$ denotes the scalar coefficient for $\hat{\pi}(\kappa|\mathbf{x}')$. $Q_S = \{\kappa \in \mathbb{N}^n | \forall i \in S, \kappa_i \in \mathbb{N}^+; \forall i \notin S, \kappa_i = 0\}$ denotes the set of degree vectors corresponding to all Taylor expansion terms involving only variables in S . Furthermore, the second-order moment of the standard AND interaction $\hat{\pi}(\kappa|\mathbf{x} + \epsilon)$ w.r.t. the Gaussian perturbations ϵ is derived as follows.

$$\forall \kappa \in Q_S, \mathbb{E}_{\epsilon}[\hat{\pi}^2(\kappa|\mathbf{x} + \epsilon)] = \prod_{i \in S} \left[1 + \sum_{m=1}^{\kappa_i} c_m V_{2m}(\epsilon_i) \right]. \quad (6)$$

where $V_{2m}(\epsilon_i) = \mathbb{E}[\epsilon_i^{2m}] > 0$, and $c_m = \binom{2\kappa_i}{2m} \frac{1}{\tau^{2m}} > 0$.

Equation (6) tells us that for a specific standard interaction $\hat{\pi}(\kappa|\mathbf{x} + \epsilon)$ subject to $\kappa \in Q_S$, its second-order moment increases along with the order $|S|$ of the concept S in a roughly exponential manner, and its mean value $\mathbb{E}_{\epsilon}[\hat{\pi}(\kappa|\mathbf{x} + \epsilon)] \approx 1$ keeps relatively stable, which is independent with the order. Therefore, we can consider that its variance $\text{Var}_{\epsilon}[\hat{\pi}(\kappa|\mathbf{x} + \epsilon)] = \mathbb{E}_{\epsilon}[\hat{\pi}^2(\kappa|\mathbf{x} + \epsilon)] - \mathbb{E}_{\epsilon}^2[\hat{\pi}(\kappa|\mathbf{x} + \epsilon)]$ also increases along with the order $|S|$ in a roughly exponential manner. Moreover, according to Equation (5), the interactive effect $I(S|\mathbf{x}')$ of the concept S is the weighted sum of all elementary terms $\hat{\pi}(\kappa|\mathbf{x} + \epsilon)$ satisfying $\kappa \in Q_S$, and different terms of $\hat{\pi}(\kappa|\mathbf{x} + \epsilon)$ w.r.t. the same set S are roughly positively correlated to each other. Therefore, we can consider that the variance of $I(S|\mathbf{x}')$ has approximately an exponent relation with the order of the concept S , i.e., $|S|$. This proves that low-order interactive concepts can be considered more stable than high-order interactive concepts.

Experimental verification. We conducted experiments to verify the exponential relation of the interactive effect's variance $\text{Var}_{\epsilon}[I(S|\mathbf{x}' = \mathbf{x} + \epsilon)]$ with the order of the concept $|S|$. To this end, given a well-trained DNN and an input sample \mathbf{x} , we added a Gaussian perturbation $\epsilon \sim \mathcal{N}(\mathbf{0}, \delta^2 \mathbf{I})$ to the input sample. Then, we used the metric $V^{(s)} = \mathbb{E}_{\mathbf{x}}[\mathbb{E}_{|S|=s}[\text{Var}_{\epsilon}[I(S|\mathbf{x} + \epsilon)]]]$ to measure the average variance of the s -th order concepts encoded by the DNN w.r.t. the Gaussian perturbation ϵ . In the implementation, we used the DNNs introduced in Section 2.2.1 for testing. Figure 8 shows that the variance $V^{(s)}$ of the interactive effect of the concept S increased along with the order s of the concept in a roughly exponential manner.

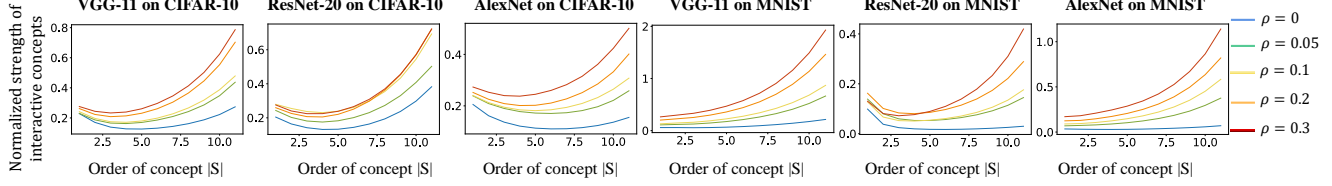


Figure 6. Normalized interaction strength of interactive concepts of different orders $\mathbb{E}_{\mathbf{x} \in D} \mathbb{E}_{S: |S|=m} \left[\frac{|I^{(m)}(S|\mathbf{x})|}{\mathbb{E}_{\mathbf{x} \in D} [v(N|\mathbf{x}) - v(\emptyset|\mathbf{x})]} \right]$. We compare interaction strength between DNNs trained with different noise levels $\rho = 0, 0.05, 0.1, 0.2, 0.3$.

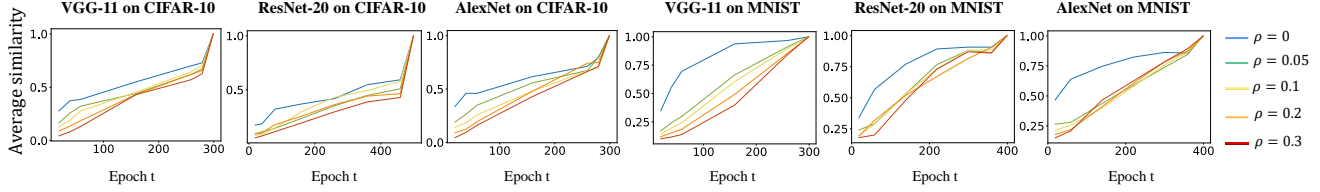


Figure 7. Average similarity $Sim^{(m=1,t)}$ between low-order interactive concepts encoded after the t -th epoch and those encoded after all epochs. We compare $Sim^{(m=1,t)}$ between DNNs trained with different noise levels ρ . Appendix C.4 shows results for 2-order concepts and 3-order concepts.

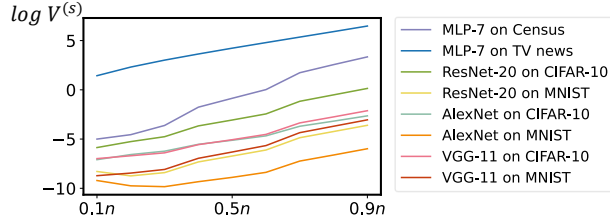


Figure 8. Logarithm of the variance. The variance of effects of interactive concepts increases along with the order exponentially.

2.3. An over-fitted DNN usually encodes strong high-order interactive concepts

In the previous subsection, we have proven that low-order interactive concepts extracted from training data can be better generalized to testing data than high-order concepts. In this subsection, we will analyze and explain the internal reason for the generalization power of the entire DNN based on the generalization power of encoded interactive concepts.

Claim1: The DNN with poor generalization power mainly encodes strong high-order interactive concepts. To verify the above claim, we trained DNNs with different generalization power, which suffered from the over-fitting problem at different levels. In this way, we examined whether the DNN with poor generalization power encoded stronger high-order interactive concepts than the DNN with strong generalization power. Specifically, we assigned a ratio ρ ($0 \leq \rho \leq 1$) of training samples with incorrect labels to train a DNN, which was termed a *DNN with ρ noise*. We considered that a DNN trained with more incorrect labels (a high ρ value) was more over-fitted. In this way, we trained DNNs with different generalization powers by applying different

ratios of incorrect labels. We trained *AlexNet*, *ResNet-20* and *VGG-11* with $\rho = 0, 0.05, 0.1, 0.2, 0.3$ noise on the MNIST dataset and the CIFAR-10 dataset. Then, for each DNN, we computed the average interaction strength of concepts of each specific order m over different training samples, i.e., $\mathbb{E}_{\mathbf{x} \in D} \mathbb{E}_{S: |S|=m} \left[\frac{|I^{(m)}(S|\mathbf{x})|}{\mathbb{E}_{\mathbf{x} \in D} [v(N|\mathbf{x}) - v(\emptyset|\mathbf{x})]} \right]$. Figure 6 shows that the DNN trained with more incorrect labels (a high ρ value) usually encoded more significant high-order concepts than the DNN trained with fewer incorrect labels. This meant that more over-fitted DNNs usually encoded stronger high-order concepts.

Claim2: The DNN with a good generalization power usually learns low-order interactive concepts more quickly. Let us focus on the interactive concepts of a specific order m . For each DNN, we considered interactive concepts encoded by the finally trained DNN v^* as the objective interactive concepts that needed to be learned. Thus, when the DNN $v^{(t)}$ was trained after t epochs, we measured the Jaccard similarity between the interactive concepts encoded by $v^{(t)}$ and final interactive concepts encoded by v^* , to evaluate the learning progress of all the m -order interactive concepts after t epochs. Specifically, we computed the Jaccard similarities between m -order interactive concepts encoded by $v^{(t)}$ and those encoded by v^* . Then we averaged such similarities over different samples, $Sim^{(m,t)} = \mathbb{E}_{\mathbf{x} \in D} [sim(\tilde{I}_t^{(m)}(\mathbf{x}), \tilde{I}^{*(m)}(\mathbf{x}))]$ as a metric for the learning progress, where $sim(\cdot)$ denoted the Jaccard similarity, and the vector $\tilde{I}_t^{(m)}(\mathbf{x})$ was defined under Equation (3) and enumerated all m -order interactive concepts extracted from sample \mathbf{x} at the epoch t . In this way, if a DNN achieved a high/low similarity $Sim^{(m,t)}$ in early epochs, then we considered that this DNN learned interactive

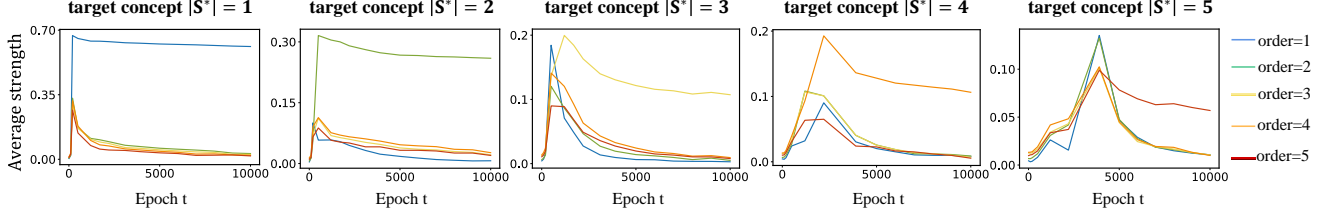


Figure 9. Average strength $\mathbb{E}_{\mathbf{x} \in X} [\sum_{S: |S|=m} |I_t^{(m)}(S|\mathbf{x})|]$ of interactive concepts of different orders.

concepts of the m -th order quickly/slowly.

Then, we conducted experiments to compare the learning speeds of interactive concepts between DNNs with different generalization powers. Experimental settings were the same as in paragraphs for Claim 1, which used different ratios ρ of noise labels to train DNNs that were over-fitted at different levels. We trained AlexNet, ResNet-20 and VGG-11 with different ratios $\rho = 0, 0.05, 0.1, 0.2, 0.3$ of incorrect labels on the MNIST dataset and the CIFAR-10 dataset. Figure 7 shows that a less over-fitted DNN usually exhibited a higher $Sim^{(m,t)}$ in early epochs for low-order interactive concepts. It meant that DNNs with a strong generalization power usually learned low-order interactive concepts more quickly.

2.4. Learning dynamics of interactive concepts

In this section, we analyze the learning dynamics of concepts as a new perspective to understand why high-order interactive concepts are more likely to be over-fitted. Specifically, we conducted experiments to compare the dynamics of a DNN learning a low-order concept with the dynamics of learning a high-order concept, so as to explain how the learning of high-order concepts was over-fitted.

We trained a DNN v to fit a random concept $S^* \subseteq N$ of the m -th order, $m = |S^*|$. Given an arbitrary input sample \mathbf{x} , if the input variable x_i was set to the original value, then we set $A_i = 1$; if the input variable was masked, then we set $A_i = 0$. Thus, the m -th order target concept was formulated as $u_{S^*}(\mathbf{x}) = \prod_{i \in S^*} A_i$. We trained the DNN to fit the function of the concept $u_{S^*}(\mathbf{x})$ based on the $Loss = \mathbb{E}_{\mathbf{x} \in X} [\|v(\mathbf{x}) - u_{S^*}(\mathbf{x})\|^2]$. The DNN was trained on a dataset $X = \{0, 1\}^n$, which contained samples corresponding to all masking states $\mathbf{x} = [x_1, x_2, \dots, x_n]^T \in X, \forall i, x_i \in \{0, 1\}$.

Then, we tracked the change in the average strength of interactive concepts of different orders over different samples, $\mathbb{E}_{\mathbf{x} \in X} [\sum_{S: |S|=m} |I_t^{(m)}(S|\mathbf{x})|]$, during the entire learning process. If a DNN had been well trained after t epochs, then it was supposed to only extract a single interactive concept with non-zero effect $I_t^{(m)}(S|\mathbf{x})$. However, in the real training process, the DNN simultaneously learned interactive concepts of different orders.

To analyze the above dynamics of learning interactive

concepts of different orders, we trained a five-layer MLP on the dataset X , $n = 10$. Figure 9 shows that when a DNN was trained to fit a low-order interactive concept (*i.e.*, the target concept S^* was of a low order), the DNN usually learned such an interactive concept directly. In comparison, when a DNN was trained to fit a high-order interactive concept, the DNN usually first learned interactive concepts of low orders. Then, the DNN shifted its attention to interactive concepts of higher orders, and later gradually removed mistakenly learned low-order interactive concepts.

In this way, we found that high-order interactive concepts were usually more difficult to be learned than low-order interactive concepts. A high-order interactive concepts was likely to be mistakenly encoded as a mixture of low-order interactive concepts. Thus, the learned high-order interactive concepts were less likely to be generalized to testing samples than low-order interactive concepts.

3. Conclusion

In this paper, we have used the interactive concept to provide a new perspective to understand the generalization power of a DNN. We find that low-order concepts in training data are usually better generalized to testing data than high-order concepts. Besides, we also find that DNNs with poor generalization power usually encode more high-order concepts than DNNs with strong generalization power. DNNs with strong generalization power usually encoded low-order concepts more quickly than other DNNs. Moreover, we have analyzed the learning dynamics for interactive concepts, and we find that low-order concepts are usually learned directly, but high-order concepts are more likely to be mistakenly encoded as a mixture of various incorrect low-order concepts in the early phase of the learning process. The removing of these incorrect low-order concepts usually takes a long time in the later learning process. Thus, the instability/difficulty of learning high-order concepts have effectively explained why high-order concepts are more difficult to be generalized to testing samples than low-order concepts.

References

Marco Ancona, Cengiz Oztireli, and Markus Gross. Explaining deep neural networks with a polynomial time

- algorithm for shapley value approximation. In *International Conference on Machine Learning*, pages 272–281. PMLR, 2019. 6
- Devansh Arpit, Stanisław Jastrzębski, Nicolas Ballas, David Krueger, Emmanuel Bengio, Maxinder S Kanwal, Tegan Maharaj, Asja Fischer, Aaron Courville, Yoshua Bengio, et al. A closer look at memorization in deep networks. In *International conference on machine learning*, pages 233–242. PMLR, 2017. 5
- Arthur Asuncion and David Newman. Uci machine learning repository, 2007. 3
- Peter L Bartlett, Dylan J Foster, and Matus J Telgarsky. Spectrally-normalized margin bounds for neural networks. *Advances in neural information processing systems*, 30, 2017. 4
- Anselm Blumer, Andrzej Ehrenfeucht, David Haussler, and Manfred K Warmuth. Occam’s razor. *Information processing letters*, 24(6):377–380, 1987. 3
- Olivier Bousquet and André Elisseeff. Stability and generalization. *The Journal of Machine Learning Research*, 2: 499–526, 2002. 12
- Olivier Bousquet, Yegor Klochkov, and Nikita Zhivotovskiy. Sharper bounds for uniformly stable algorithms. In *Conference on Learning Theory*, pages 610–626. PMLR, 2020. 4, 12
- Yuheng Bu, Shaofeng Zou, and Venugopal V Veeravalli. Tightening mutual information-based bounds on generalization error. *IEEE Journal on Selected Areas in Information Theory*, 1(1):121–130, 2020. 12
- Yuan Cao and Quanquan Gu. Generalization error bounds of gradient descent for learning over-parameterized deep relu networks. In *Proceedings of the AAAI Conference on Artificial Intelligence*, volume 34, pages 3349–3356, 2020. 12
- Piotr Dabkowski and Yarin Gal. Real time image saliency for black box classifiers. *Advances in neural information processing systems*, 30, 2017. 3
- Huiqi Deng, Qihan Ren, Hao Zhang, and Quanshi Zhang. Discovering and explaining the representation bottleneck of dnns. In *International Conference on Learning Representations*, 2021a. 1, 2, 3
- Zhun Deng, Hangfeng He, and Weijie Su. Toward better generalization bounds with locally elastic stability. In *International Conference on Machine Learning*, pages 2590–2600. PMLR, 2021b. 4, 12
- Gintare Karolina Dziugaite and Daniel M Roy. Computing nonvacuous generalization bounds for deep (stochastic) neural networks with many more parameters than training data. In *Association for Uncertainty in Artificial Intelligence*, 2017a. 12
- Gintare Karolina Dziugaite and Daniel M Roy. Computing nonvacuous generalization bounds for deep (stochastic) neural networks with many more parameters than training data. *arXiv preprint arXiv:1703.11008*, 2017b. 1, 4
- Vitaly Feldman and Jan Vondrak. Generalization bounds for uniformly stable algorithms. *Advances in Neural Information Processing Systems*, 31, 2018. 12
- Vitaly Feldman and Jan Vondrak. High probability generalization bounds for uniformly stable algorithms with nearly optimal rate. In *Conference on Learning Theory*, pages 1270–1279. PMLR, 2019. 12
- Pierre Foret, Ariel Kleiner, Hossein Mobahi, and Behnam Neyshabur. Sharpness-aware minimization for efficiently improving generalization. In *International Conference on Learning Representations*, 2021. 4, 12
- Stanislav Fort, Paweł Krzysztof Nowak, Stanisław Jastrzebski, and Sridhar Narayanan. Stiffness: A new perspective on generalization in neural networks. *arXiv preprint arXiv:1901.09491*, 2019. 1
- Michel Grabisch and Marc Roubens. An axiomatic approach to the concept of interaction among players in cooperative games. *International Journal of game theory*, 28(4):547–565, 1999. 14
- Mahdi Haghifam, Jeffrey Negrea, Ashish Khisti, Daniel M Roy, and Gintare Karolina Dziugaite. Sharpened generalization bounds based on conditional mutual information and an application to noisy, iterative algorithms. *Advances in Neural Information Processing Systems*, 33:9925–9935, 2020. 4, 12
- Mahdi Haghifam, Gintare Karolina Dziugaite, Shay Moran, and Dan Roy. Towards a unified information-theoretic framework for generalization. *Advances in Neural Information Processing Systems*, 34:26370–26381, 2021. 4, 12
- John C Harsanyi. A simplified bargaining model for the n-person cooperative game. In *Papers in game theory*, pages 44–70. Springer, 1982. 3
- Kaiming He, Xiangyu Zhang, Shaoqing Ren, and Jian Sun. Deep residual learning for image recognition. In *Proceedings of the IEEE conference on computer vision and pattern recognition*, pages 770–778, 2016. 3

- Andrew Ilyas, Shibani Santurkar, Dimitris Tsipras, Logan Engstrom, Brandon Tran, and Aleksander Madry. Adversarial examples are not bugs, they are features. *Advances in neural information processing systems*, 32, 2019. 5
- Stanislaw Jastrzebski, Devansh Arpit, Oliver Astrand, Giancarlo B Kerg, Huan Wang, Caiming Xiong, Richard Socher, Kyunghyun Cho, and Krzysztof J Geras. Catastrophic fisher explosion: Early phase fisher matrix impacts generalization. In *International Conference on Machine Learning*, pages 4772–4784. PMLR, 2021. 12
- Yiding Jiang, Behnam Neyshabur, Hossein Mobahi, Dilip Krishnan, and Samy Bengio. Fantastic generalization measures and where to find them. In *International Conference on Learning Representations*, 2020. 12
- Nitish Shirish Keskar, Dheevatsa Mudigere, Jorge Nocedal, Mikhail Smelyanskiy, and Ping Tak Peter Tang. On large-batch training for deep learning: Generalization gap and sharp minima. *arXiv preprint arXiv:1609.04836*, 2016. 1, 4
- Nitish Shirish Keskar, Dheevatsa Mudigere, Jorge Nocedal, Mikhail Smelyanskiy, and Ping Tak Peter Tang. On large-batch training for deep learning: Generalization gap and sharp minima. In *International Conference on Learning Representations*, 2017. 12
- Alex Krizhevsky, Geoffrey Hinton, et al. Learning multiple layers of features from tiny images. 2009. 3, 5
- Alex Krizhevsky, Ilya Sutskever, and Geoffrey E Hinton. Imagenet classification with deep convolutional neural networks. *Communications of the ACM*, 60(6):84–90, 2017. 3
- Jungmin Kwon, Jeongseop Kim, Hyunseo Park, and In Kwon Choi. Asam: Adaptive sharpness-aware minimization for scale-invariant learning of deep neural networks. In *International Conference on Machine Learning*, pages 5905–5914. PMLR, 2021. 4, 12
- Yann LeCun, Léon Bottou, Yoshua Bengio, and Patrick Haffner. Gradient-based learning applied to document recognition. *Proceedings of the IEEE*, 86(11):2278–2324, 1998. 3
- Benjamin J Lengerich, Eric Xing, and Rich Caruana. Dropout as a regularizer of interaction effects. In *International Conference on Artificial Intelligence and Statistics*, pages 7550–7564. PMLR, 2022. 12
- Hao Li, Zheng Xu, Gavin Taylor, Christoph Studer, and Tom Goldstein. Visualizing the loss landscape of neural nets. *Advances in neural information processing systems*, 31, 2018. 4, 12
- Harsh Mehta, Ashok Cutkosky, and Behnam Neyshabur. Extreme memorization via scale of initialization. In *International Conference on Learning Representations*, 2020. 12
- Jeffrey Negrea, Mahdi Haghifam, Gintare Karolina Dziugaite, Ashish Khisti, and Daniel M Roy. Information-theoretic generalization bounds for sgld via data-dependent estimates. *Advances in Neural Information Processing Systems*, 32, 2019. 12
- Behnam Neyshabur, Ryota Tomioka, and Nathan Srebro. Norm-based capacity control in neural networks. In *Conference on Learning Theory*, pages 1376–1401. PMLR, 2015. 1
- Behnam Neyshabur, Srinadh Bhojanapalli, David McAllester, and Nati Srebro. Exploring generalization in deep learning. *Advances in neural information processing systems*, 30, 2017. 4
- Jie Ren, Mingjie Li, Qihan Ren, Huiqi Deng, and Quanshi Zhang. Towards axiomatic, hierarchical, and symbolic explanation for deep models. *arXiv preprint arXiv:2111.06206*, 2021. 1, 2, 3, 12
- Jie Ren, Zhanpeng Zhou, Qirui Chen, and Quanshi Zhang. Can we faithfully represent absence states to compute shapley values on a dnn? In *11th International Conference on Learning Representations, ICLR 2022*, 2022. URL <https://openreview.net/forum?id=YV8tP7bW6Kt>. 1, 2, 3
- Daniel Russo and James Zou. How much does your data exploration overfit? controlling bias via information usage. *IEEE Transactions on Information Theory*, 66(1):302–323, 2019. 12
- Karen Simonyan and Andrew Zisserman. Very deep convolutional networks for large-scale image recognition. *arXiv preprint arXiv:1409.1556*, 2014. 3
- Thomas Steinke and Lydia Zakyntinou. Reasoning about generalization via conditional mutual information. In *Conference on Learning Theory*, pages 3437–3452. PMLR, 2020. 12
- Mukund Sundararajan, Kedar Dhamdhere, and Ashish Agarwal. The shapley taylor interaction index. In *International conference on machine learning*, pages 9259–9268. PMLR, 2020. 12
- Hao Wang, Yizhe Huang, Rui Gao, and Flavio Calmon. Analyzing the generalization capability of sgld using properties of gaussian channels. *Advances in Neural Information Processing Systems*, 34:24222–24234, 2021. 12

Tsui-Wei Weng, Huan Zhang, Pin-Yu Chen, Jinfeng Yi, Dong Su, Yupeng Gao, Cho-Jui Hsieh, and Luca Daniel. Evaluating the robustness of neural networks: An extreme value theory approach. *arXiv preprint arXiv:1801.10578*, 2018. 1

Sen Wu, Hongyang Zhang, Gregory Valiant, and Christopher Ré. On the generalization effects of linear transformations in data augmentation. In *International Conference on Machine Learning*, pages 10410–10420. PMLR, 2020. 12

Aolin Xu and Maxim Raginsky. Information-theoretic analysis of generalization capability of learning algorithms. *Advances in Neural Information Processing Systems*, 30, 2017. 12

Hao Zhang, Sen Li, Yinchao Ma, Mingjie Li, Yichen Xie, and Quanshi Zhang. Interpreting and boosting dropout from a game-theoretic view. In *International Conference on Learning Representations*, 2021a. 12

Linjun Zhang, Zhun Deng, Kenji Kawaguchi, Amirata Ghorbani, and James Zou. How does mixup help with robustness and generalization? In *International Conference on Learning Representations*, 2021b. 12

A. Previous studies on generalization power of DNNs

Many previous studies have tried to explain and analyze the generalization power of the DNN. These previous studies mainly considered the following perspectives.

Deriving the generalization bound of DNNs. For a given DNN and dataset, the discrepancy between the empirical error (training error) and the population error (testing error) measures the generalization error of the DNN. A line of researches have studied the upper bound of the generalization error, which is termed as the generalization bound. The *uniform stability* Bousquet and Elisseeff [2002] derived a strong exponential generalization bound by considering whether a DNN is sensitive to the deletion of a single data point. Many studies Feldman and Vondrak [2018, 2019], Bousquet et al. [2020], Deng et al. [2021b] further developed this generalization bound from different perspectives. Furthermore, many generalization bounds have been derived according to the connection between the geometry (e.g., sharpness) of the loss landscape and the generalization power Keskar et al. [2017], Dziugaite and Roy [2017a], Li et al. [2018], Jiang et al. [2020]. Based on these generalization bounds, Foret et al. [2021], Kwon et al. [2021] further proposed a sharpness-aware minimization procedure to efficiently improve model generalization, by simultaneously minimizing the training loss and the sharpness of the loss landscape. In addition, extensive studies Xu and Raginsky [2017], Russo and Zou [2019], Negrea et al. [2019], Bu et al. [2020] have used the (unconditional) mutual information between the DNN and the training dataset as an indicator of the generalization performance. Later, Steinke and Zakynthinou [2020] proposed the conditional mutual information framework, which has been shown capable to derive tighter generalization bounds than those based on the unconditional mutual information Haghifam et al. [2020, 2021].

Explaining the effect of optimization on the generalization. It has been widely investigated that the optimization of a DNN has a dramatic effect on its generalization power. Cao and Gu [2020], Mehta et al. [2020], Jastrzebski et al. [2021] explained why the commonly used stochastic gradient descent (SGD) optimization can avoid a poor generalization from different perspectives. Wang et al. [2021] analyzed the generalization capacity of using the stochastic gradient Langevin dynamics (SGLD) optimization and the differentially private SGD (DP-SGD) optimization. Besides, Zhang et al. [2021a], Lengerich et al. [2022] explained the effect of the dropout on the generalization from the perspective of interaction effects between input variables, but failed to explain the connection between the interaction and the generalization power of a DNN. Wu et al. [2020], Zhang et al. [2021b] proved the regularization effect of the typical Mixup augmentation on the generalization power.

Unlike previous studies, we analyze and explain the generalization power of the DNN from a new perspective, i.e., interactive concepts that a DNN encodes.

B. Properties for the Harsanyi dividend

We used the Harsanyi dividend to measure the numerical effect $I(S|\mathbf{x})$ of the interactive concept S as introduced in Section 2.1. Ren et al. [2021] have proven that the Harsanyi dividend satisfied the following properties, including the *efficiency, linearity, dummy, symmetry, anonymity, recursive, interaction distribution properties*.

(1) Efficiency property: The output score of a model $v(\mathbf{x})$ can be decomposed into the interactive effects of different interactive concepts $I(S|\mathbf{x})$, $S \subseteq N$, i.e., $v(\mathbf{x}) = \sum_{S \subseteq N} I(S|\mathbf{x})$.

(2) Linearity property: if the output score of the model u and the output score of the model v is merged as the output score of the model w , i.e., $\forall S \subseteq N, w(\mathbf{x}_S) = u(\mathbf{x}_S) + v(\mathbf{x}_S)$, then their interactive effects $I_u(S|\mathbf{x})$ and $I_v(S|\mathbf{x})$ can be merged as $I_w(S|\mathbf{x})$, i.e., $\forall S \subseteq N, I_w(S|\mathbf{x}) = I_u(S|\mathbf{x}) + I_v(S|\mathbf{x})$.

(3) Dummy property: If the variable i is considered as a dummy variable, i.e., $\forall S \subseteq N \setminus \{i\}, v(\mathbf{x}_{S \cup \{i\}}) = v(\mathbf{x}_S) + v(\mathbf{x}_{\{i\}})$, then this variable i has no interaction with other variables, i.e., $\forall \emptyset \neq S \subseteq N \setminus \{i\}, I(S \cup \{i\}|\mathbf{x}) = 0$.

(4) Symmetry property: If two input variable $i, j \in N$ cooperate with other input variables in $S \subseteq N \setminus \{i, j\}$ in the same way, i.e., $\forall S \subseteq N \setminus \{i, j\}, v(\mathbf{x}_{S \cup \{i\}}) = v(\mathbf{x}_{S \cup \{j\}})$, then these two input variables have the same interactive effects, i.e., $\forall S \subseteq N \setminus \{i, j\}, I(S \cup \{i\}|\mathbf{x}) = I(S \cup \{j\}|\mathbf{x})$.

(5) Anonymity property: If a random permutation π is added to N , then $\forall S \subseteq N, I_v(S|\mathbf{x}) = I_{\pi v}(\pi S|\mathbf{x})$ is always guaranteed, where the new set of input variables πS is defined as $\pi S = \{\pi(i), i \in S\}$, the new model πv is defined as $(\pi v)(\mathbf{x}_{\pi S}) = v(\mathbf{x}_S)$. This suggests that permutation does not change the interactive effects.

(6) Recursive property: The interactive effects can be calculated in a recursive manner. For $\forall i \in N, S \subseteq N \setminus \{i\}$, the interactive effects of $S \cup \{i\}$ can be computed as the difference between the interactive effects of S with the presence of the variable i and the interactive effects of S with the absence of the variable i . I.e., $\forall i \in N, S \subseteq N \setminus \{i\}, I(S \cup \{i\}|\mathbf{x}) = I(S|i \text{ is consistently present}, \mathbf{x}) - I(S|\mathbf{x})$, where $I(S|i \text{ is consistently present}, \mathbf{x}) = \sum_{L \subseteq S} (-1)^{|S|-|L|} v(\mathbf{x}_{L \cup \{i\}})$.

(7) Interaction distribution property: This property describes how an interaction function Sundararajan et al. [2020] distributes interactions. An interaction function v_T parameterized by a context T is defined as follows, i.e., $\forall S \subseteq N$, if context

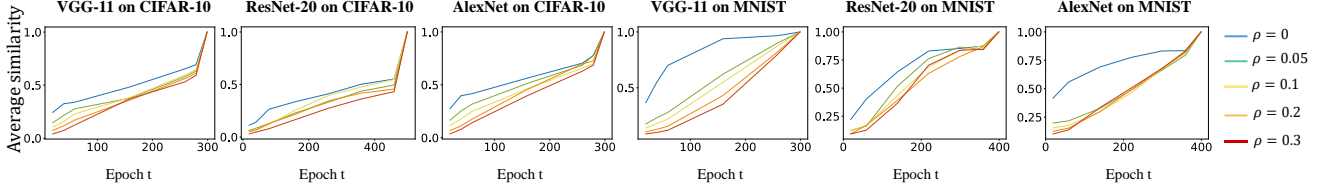


Figure 10. Average similarity $Sim^{(m=2,t)}$ between 2-order concepts encoded after the t -th epoch and those encoded after all epochs. We compare $Sim^{(m=2,t)}$ between DNNs trained with different noise levels ρ .

T is a subset of S , i.e., $T \subseteq S$, then $v_T(\mathbf{x}_S) = c$; if not, $v_T(\mathbf{x}_S) = 0$. Then, the interactive effects for an interaction function v_T can be computed as, $I(T|\mathbf{x}) = c$, and $\forall S \neq T, I(S|\mathbf{x}) = 0$.

C. More experimental details and results

C.1. Simplifying the computation of interaction

As discussed in Section 2.1, there are 2^n possible interactive concepts S for an input sample \mathbf{x} with n input variables. Thus, the computational cost for $I(S|\mathbf{x})$ is huge when n is large. Therefore, we sample some image patches for each input sample, and each image patch is considered to be an input variable.

- For MNIST dataset, we resize the input image from 28×28 to 32×32 , and split the input image (32×32) into 8×8 patches. We manually sample 12 image patches that contain the foreground information, and regard each image patch as an input variable, all the remaining image patches are masked with the baseline value.

- For CIFAR-10 dataset, we split the input image (32×32) into 8×8 patches. We randomly select 12 patches, and regard each image patch as an input variable, all the remaining image patches are masked with the baseline value.

C.2. Experimental details in computing $\log V^{(s)}$

In this section, we show more experimental details about the experiment in Figure 8.

- For tabular data, i.e., the census dataset and the TV news dataset, we randomly sample 50 training samples from each class. In order to mimic the variation in data, we add a Gaussian perturbation $\epsilon \sim \mathcal{N}(\mathbf{0}, \delta^2 \mathbf{I})$ to each training sample, where $\delta = 0.05$. For each training sample \mathbf{x} , we sample 20 perturbed sample $\mathbf{x}' = \mathbf{x} + \epsilon$. We set $\tau = 0.5$, in this way, we set the baseline value $b_i = x_i + \tau$, if $x_i < \mu_i$; and set $b_i = x_i - \tau$, if $x_i > \mu_i$.

- For image data, i.e., the CIFAR-10 dataset and the MNIST dataset, we randomly sample 10 training samples from each class. In order to mimic the variation in data, we add a Gaussian perturbation $\epsilon \sim \mathcal{N}(\mathbf{0}, \delta^2 \mathbf{I})$ to each training sample, where $\delta = 0.02$. For each training sample \mathbf{x} , we sample 20 perturbed sample $\mathbf{x}' = \mathbf{x} + \epsilon$. We set $\tau = 2$, in this way, we set the baseline value $b_i = x_i + \tau$, if $x_i < \mu_i$; and set $b_i = x_i - \tau$, if $x_i > \mu_i$.

C.3. Experimental details in Section 2.3

- In Claim 1, for each DNN, e.g., AlexNet with $\rho = 0.05$ noise on the CIFAR-10 dataset, we randomly sample 2 training samples from each class. Then, we compute the average normalized interaction strength of interactive concepts of each specific order m over 20 training samples, i.e., $\mathbb{E}_{\mathbf{x} \in D} \mathbb{E}_{S: |S|=m} \left[\frac{|I^{(m)}(S|\mathbf{x})|}{\mathbb{E}_{\mathbf{x} \in D} [v(N|\mathbf{x}) - v(\emptyset|\mathbf{x})]} \right]$. We trained 10 DNNs with different initialization parameters by setting 10 different seeds, respectively. Then, we average the normalized interaction strengths over these 10 different DNNs.

- In Claim 2, for each DNN, e.g., AlexNet with $\rho = 0.05$ noise on the CIFAR-10 dataset, we randomly sample 40 training samples, we compute the average similarity over these 40 training samples, i.e., $Sim^{(m,t)} = \mathbb{E}_{\mathbf{x} \in D} [sim(\tilde{I}_t^{(m)}(\mathbf{x}), \tilde{I}^{*(m)}(\mathbf{x}))]$. We trained 10 DNNs with different initialization parameters by setting 10 different seeds, respectively. Then, we average the similarities over these 10 different DNNs.

C.4. More experimental results for learning speed of low-order interactive concepts

As a supplement to Figure 7, Section 2.3 of the paper, in this section, we show the learning speed of 2-order concepts and 3-order concepts, i.e., the average similarity $Sim^{(m,t)} (m = 2, m = 3)$ between low-order interactive concepts encoded after the t -th epoch and those encoded after all epochs.

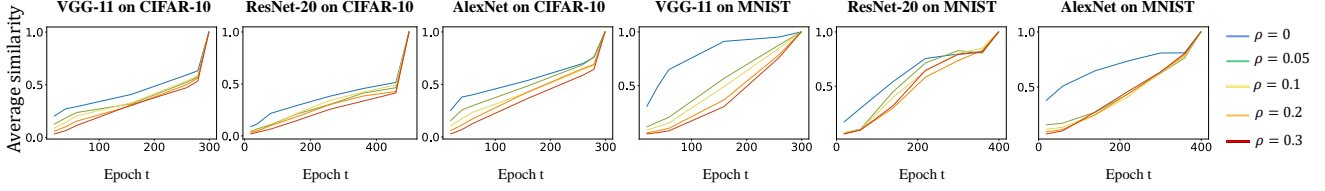


Figure 11. Average similarity $Sim^{(m=3,t)}$ between 3-order concepts encoded after the t -th epoch and those encoded after all epochs. We compare $Sim^{(m=3,t)}$ between DNNs trained with different noise levels ρ .

D. Proof of Lemmas and Theorems

Lemma 1. Given a neural network v and an arbitrary perturbed input sample $\mathbf{x}' = \mathbf{x} + \epsilon$, the neural network output $v(\mathbf{x}')$ can be rewritten by following the Taylor series expansion at the baseline point $\mathbf{b} = [b_1, \dots, b_n]^T$,

$$v(\mathbf{x}') = v(\mathbf{b}) + \sum_{k=1}^{\infty} \sum_{\boldsymbol{\kappa} \in O_k} C(\boldsymbol{\kappa}) \cdot \nabla_v(\boldsymbol{\kappa}) \cdot \pi(\boldsymbol{\kappa}|\mathbf{x}'), \quad (7)$$

including the coefficient $C(\boldsymbol{\kappa}) = \frac{1}{(\kappa_1 + \dots + \kappa_n)!} \binom{\kappa_1 + \dots + \kappa_n}{\kappa_1, \dots, \kappa_n} \in \mathbb{R}$, the partial derivative $\nabla_v(\boldsymbol{\kappa}) = \frac{\partial^{\kappa_1 + \dots + \kappa_n} v(\mathbf{b})}{\partial^{\kappa_1} x_1 \dots \partial^{\kappa_n} x_n} \in \mathbb{R}$, and the expansion term $\pi(\boldsymbol{\kappa}|\mathbf{x}') = \prod_{i=1}^n (x'_i - b_i)^{\kappa_i}$. Here, $\boldsymbol{\kappa} = [\kappa_1, \dots, \kappa_n] \in \mathbb{N}^n$ denotes the non-negative integer degree vector of each Taylor expansion term. Correspondingly, $O_k = \{\boldsymbol{\kappa} \in \mathbb{N}^n | \kappa_1 + \dots + \kappa_n = k\}$ represents the set of all expansion terms of the k -th order.

Proof. Let us expand the output $v(\mathbf{x}')$ of the perturbed input sample at the baseline point $\mathbf{b} = [b_1, \dots, b_n]^T$. It is easy to obtain Eq. (7) according to the Taylor series expansion. \square

Theorem 2. Given a neural network v and an arbitrary perturbed input sample $\mathbf{x}' = \mathbf{x} + \epsilon$ by adding a Gaussian perturbation $\epsilon \sim \mathcal{N}(\mathbf{0}, \delta^2 \mathbf{I})$, the interactive effect $I(S|\mathbf{x}')$ is defined by setting $(\mathbf{x}'_T)_i = x'_i$ if $i \in T$ and setting $(\mathbf{x}'_T)_i = b_i$ if $i \notin T$. Then, we obtain

$$\begin{aligned} I(S|\mathbf{x}') &= \sum_{\boldsymbol{\kappa} \in Q_S} C(\boldsymbol{\kappa}) \cdot \nabla_v(\boldsymbol{\kappa}) \cdot \pi(\boldsymbol{\kappa}|\mathbf{x}') \\ &= \sum_{\boldsymbol{\kappa} \in Q_S} Z(\boldsymbol{\kappa}) \cdot \hat{\pi}(\boldsymbol{\kappa}|\mathbf{x}') \end{aligned} \quad (8)$$

where $\hat{\pi}(\boldsymbol{\kappa}|\mathbf{x}') = \prod_{i=1}^n \left(\frac{\text{sign}(x_i - b_i)}{\tau} \right)^{\kappa_i} \cdot \pi(\boldsymbol{\kappa}|\mathbf{x}')$ is a standard AND interaction of the degree vector $\boldsymbol{\kappa}$, which is normalized to satisfy $\forall \boldsymbol{\kappa} \in Q_S, \mathbb{E}_{\epsilon}[\hat{\pi}(\boldsymbol{\kappa}|\mathbf{x}' = \mathbf{x} + \epsilon)] = 1 + O(\delta^2)$. In addition, $Z(\boldsymbol{\kappa}) = \prod_{i=1}^n \left(\frac{\tau}{\text{sign}(x_i - b_i)} \right)^{\kappa_i} \cdot C(\boldsymbol{\kappa}) \cdot \nabla_v(\boldsymbol{\kappa})$ denotes the scalar coefficient for $\hat{\pi}(\boldsymbol{\kappa}|\mathbf{x}')$. $Q_S = \{\boldsymbol{\kappa} \in \mathbb{N}^n | \forall i \in S, \kappa_i \in \mathbb{N}^+; \forall i \notin S, \kappa_i = 0\}$ denotes the set of degree vectors corresponding to all Taylor expansion terms involving only variables in S . Furthermore, the second-order moment of the standard AND interaction $\hat{\pi}(\boldsymbol{\kappa}|\mathbf{x} + \epsilon)$ w.r.t. the Gaussian perturbations ϵ is derived as follows.

$$\forall \boldsymbol{\kappa} \in Q_S, \mathbb{E}_{\epsilon}[\hat{\pi}^2(\boldsymbol{\kappa}|\mathbf{x} + \epsilon)] = \prod_{i \in S} \left[1 + \sum_{m=1}^{\kappa_i} c_m V_{2m}(\epsilon_i) \right]. \quad (9)$$

where $V_{2m}(\epsilon_i) = \mathbb{E}(\epsilon_i^{2m}) > 0$ denotes the $2m$ -order moment of the variable ϵ_i , and its coefficient $c_m = \binom{2\kappa_i}{2m} \frac{1}{\tau^{2m}} > 0$ is a positive constant.

Proof. • First, let us prove Eq. (8). Let us denote the function on the right of Eq. (8) by $\tilde{I}(S|\mathbf{x}')$, i.e.,

$$\tilde{I}(S|\mathbf{x}') = \sum_{\boldsymbol{\kappa} \in Q_S} C(\boldsymbol{\kappa}) \cdot \nabla_v(\boldsymbol{\kappa}) \cdot \pi(\boldsymbol{\kappa}|\mathbf{x}') \quad (10)$$

We need to prove that for any arbitrary perturbed input sample $\forall \mathbf{x}' \in \mathbb{R}^n$, $\tilde{I}(S|\mathbf{x}') = I(S|\mathbf{x}')$.

Actually, it has been proven in [Grabisch and Roubens \[1999\]](#) that the Harsanyi dividend interaction $I(S|\mathbf{x}')$ is the **unique** metric satisfying the following faithfulness requirement,

$$\forall T \subseteq N, v(\mathbf{x}'_T) = \sum_{S \subseteq T} I(S|\mathbf{x}'). \quad (11)$$

where \mathbf{x}'_T represents a masked input sample, where input variables in $N \setminus T$ are masked with their baseline values b_i . Thus, as long as we can prove that $\tilde{I}(S|\mathbf{x}')$ also satisfies the faithfulness requirement, we can obtain $\tilde{I}(S|\mathbf{x}') = I(S|\mathbf{x}')$.

To this end, we only need to prove $\tilde{I}(S|\mathbf{x}')$ also satisfies the faithfulness requirement in Eq. (11). Specifically, given an input sample $\forall \mathbf{x}' \in \mathbb{R}^n$, let us consider the Taylor expansion of the network output $v(\mathbf{x}'_T)$ of an arbitrarily masked sample $\mathbf{x}'_T (\forall T \subseteq N)$, which is expanded at the baseline point $\mathbf{b} = [b_1, \dots, b_n]^T$. Then, according to Lemma 1,

$$\begin{aligned} \forall T \subseteq N, \quad v(\mathbf{x}'_T) &= v(\mathbf{b}) + \sum_{k=1}^{\infty} \sum_{\boldsymbol{\kappa} \in O_k} C(\boldsymbol{\kappa}) \cdot \nabla_v(\boldsymbol{\kappa}) \cdot \pi(\boldsymbol{\kappa}|\mathbf{x}') = \sum_{k=0}^{\infty} \sum_{\boldsymbol{\kappa} \in O_k} C(\boldsymbol{\kappa}) \cdot \nabla_v(\boldsymbol{\kappa}) \cdot \pi(\boldsymbol{\kappa}|\mathbf{x}'), \\ &= \sum_{\kappa_1=0}^{\infty} \sum_{\kappa_2=0}^{\infty} \cdots \sum_{\kappa_n=0}^{\infty} C(\boldsymbol{\kappa}) \cdot \nabla_v(\boldsymbol{\kappa}) \cdot \pi(\boldsymbol{\kappa}|\mathbf{x}'), \end{aligned} \quad (12)$$

where $\boldsymbol{\kappa} \in \{[\kappa_1, \dots, \kappa_n] | \forall i \in N, \kappa_i \in \mathbb{N}\}$ denotes the degree vector of Taylor expansion terms. In addition, b_i denotes the baseline value to mask the input variable x_i .

According to the definition of the masked sample \mathbf{x}'_T , we have that all variables in T keep unchanged and other variables are masked to the baseline value. That is, $\forall i \in T, (\mathbf{x}'_T)_i = x_i; \forall i \notin T, (\mathbf{x}'_T)_i = b_i$. Hence, we obtain $\forall i \notin T, [(\mathbf{x}'_T)_i - b_i]^{\kappa_i} = 0$. Then, among all Taylor expansion terms, only terms corresponding to degrees $\boldsymbol{\kappa}$ in the set $P = \{[\kappa_1, \dots, \kappa_n] | \forall i \in T, \kappa_i \in \mathbb{N}; \forall i \notin T, \kappa_i = 0\}$ may not be zero. Therefore, Eq. (12) can be re-written as

$$\forall T \subseteq N, \quad v(\mathbf{x}'_T) = \sum_{\boldsymbol{\pi} \in P} C(\boldsymbol{\kappa}) \cdot \nabla_v(\boldsymbol{\kappa}) \cdot \pi(\boldsymbol{\kappa}|\mathbf{x}') \quad (13)$$

We find that the set P can be divided into multiple *disjoint* sets as follows, $P = \cup_{S \subseteq T} Q_S$, where $Q_S = \{\boldsymbol{\kappa} \in \mathbb{N}^n | \forall i \in S, \kappa_i \in \mathbb{N}^+; \forall i \notin S, \kappa_i = 0\}$. Then, we can derive that

$$\forall T \subseteq N, \quad v(\mathbf{x}'_T) = \sum_{S \subseteq T} \sum_{\boldsymbol{\kappa} \in Q_S} C(\boldsymbol{\kappa}) \cdot \nabla_v(\boldsymbol{\kappa}) \cdot \pi(\boldsymbol{\kappa}|\mathbf{x}') = \sum_{S \subseteq T} \tilde{I}(S|\mathbf{x}'). \quad (14)$$

That is, $\tilde{I}(S|\mathbf{x}')$ satisfies the faithfulness requirement in Eq. (11). Therefore, the conclusion holds, *i.e.*, $I(S|\mathbf{x}') = \sum_{\boldsymbol{\kappa} \in Q_S} C(\boldsymbol{\kappa}) \cdot \nabla_v(\boldsymbol{\kappa}) \cdot \pi(\boldsymbol{\kappa}|\mathbf{x}')$. Furthermore, let us define $Z(\boldsymbol{\kappa}) = \prod_{i=1}^n (\frac{\tau}{\text{sign}(x_i - b_i)})^{\kappa_i} \cdot C(\boldsymbol{\kappa}) \cdot \nabla_v(\boldsymbol{\kappa})$ and $\hat{\pi}(\boldsymbol{\kappa}|\mathbf{x}') = \prod_{i=1}^n (\frac{\text{sign}(x_i - b_i)}{\tau})^{\kappa_i} \cdot \pi(\boldsymbol{\kappa}|\mathbf{x}')$, we can obtain that

$$I(S|\mathbf{x}') = \sum_{\boldsymbol{\kappa} \in Q_S} C(\boldsymbol{\kappa}) \cdot \nabla_v(\boldsymbol{\kappa}) \cdot \pi(\boldsymbol{\kappa}|\mathbf{x}') = \sum_{\boldsymbol{\kappa} \in Q_S} Z(\boldsymbol{\kappa}) \cdot \hat{\pi}(\boldsymbol{\kappa}|\mathbf{x}'). \quad (15)$$

• Next, let us estimate the mean value and the second-order moment of $\hat{\pi}(\boldsymbol{\kappa}|\mathbf{x}') = \mathbf{x} + \boldsymbol{\epsilon}$ *w.r.t.* the Gaussian perturbation $\boldsymbol{\epsilon} \sim \mathcal{N}(\mathbf{0}, \delta^2 \mathbf{I})$. The standard AND interaction $\hat{\pi}(\boldsymbol{\kappa}|\mathbf{x} + \boldsymbol{\epsilon})$ can be re-written as follows.

$$\begin{aligned} \hat{\pi}(\boldsymbol{\kappa}|\mathbf{x} + \boldsymbol{\epsilon}) &= \prod_{i=1}^n \left(\frac{\text{sign}(x_i - b_i)}{\tau} \right)^{\kappa_i} \cdot (x_i + \epsilon_i - b_i)^{\kappa_i} \\ &= \prod_{i=1}^n \left[\text{sign}(x_i - b_i) \cdot \frac{x_i + \epsilon_i - b_i}{\tau} \right]^{\kappa_i} \\ &= \prod_{i=1}^n \left(\text{sign}(x_i - b_i) \cdot \left[\frac{x_i - b_i}{\tau} + \frac{\epsilon_i}{\tau} \right] \right)^{\kappa_i} \\ &= \prod_{i=1}^n \left(1 + \left[\text{sign}(x_i - b_i) \cdot \frac{\epsilon_i}{\tau} \right] \right)^{\kappa_i} \end{aligned} \quad (16)$$

Let us define $\tilde{\epsilon}_i = \text{sign}(x_i - b_i) \cdot \frac{\epsilon_i}{\tau}$. Then,

$$\forall \boldsymbol{\kappa} \in Q_S, \quad \hat{\pi}(\boldsymbol{\kappa}|\mathbf{x} + \boldsymbol{\epsilon}) = \prod_{i=1}^n (1 + \tilde{\epsilon}_i)^{\kappa_i} = \prod_{i \in S} (1 + \tilde{\epsilon}_i)^{\kappa_i} \quad (17)$$

By conducting the first-order Taylor expansion of $(1 + \tilde{\epsilon}_i)^{\kappa_i}$, we can obtain when $\kappa_i \geq 1$, $(1 + \tilde{\epsilon}_i)^{\kappa_i} = 1 + \kappa_i \tilde{\epsilon}_i + O(\tilde{\epsilon}_i^2)$. In this way,

$$\begin{aligned} \mathbb{E}_{\boldsymbol{\epsilon}}(1 + \tilde{\epsilon}_i)^{\kappa_i} &= \mathbb{E}_{\boldsymbol{\epsilon}}[1 + \kappa_i \tilde{\epsilon}_i + O(\tilde{\epsilon}_i^2)] \\ &= 1 + O(\mathbb{E}_{\boldsymbol{\epsilon}}[\tilde{\epsilon}_i^2]) = 1 + O(\delta^2). \end{aligned} \quad (18)$$

Accordingly, considering that different dimensions of the perturbation are independent to each other, the **mean value** of $\hat{\pi}(\boldsymbol{\kappa}|\mathbf{x} + \boldsymbol{\epsilon})$ is given as

$$\begin{aligned}\mathbb{E}_{\boldsymbol{\epsilon}}[\hat{\pi}(\boldsymbol{\kappa}|\mathbf{x} + \boldsymbol{\epsilon})] &= \mathbb{E}_{\boldsymbol{\epsilon}}[\prod_{i \in S} (1 + \tilde{\epsilon}_i)^{\kappa_i}] = \prod_{i \in S} \mathbb{E}_{\boldsymbol{\epsilon}}[(1 + \tilde{\epsilon}_i)^{\kappa_i}] \\ &= \prod_{i \in S} [1 + O(\delta^2)] = 1 + O(\delta^2).\end{aligned}\tag{19}$$

Next, let us estimate the second-order moment of $\hat{\pi}(\boldsymbol{\kappa}|\mathbf{x} + \boldsymbol{\epsilon})$. It is easy to obtain that

$$\begin{aligned}\mathbb{E}_{\boldsymbol{\epsilon}}[(1 + \tilde{\epsilon}_i)^{2\kappa_i}] &= \mathbb{E}_{\boldsymbol{\epsilon}}[1 + \sum_{m=1}^{2\kappa_i} \binom{2\kappa_i}{m} \tilde{\epsilon}_i^m] \\ &= 1 + \sum_{m=1}^{2\kappa_i} \binom{2\kappa_i}{m} \mathbb{E}_{\boldsymbol{\epsilon}}[\tilde{\epsilon}_i^m]\end{aligned}\tag{20}$$

Since $\forall i \in N, \mathbb{E}_{\boldsymbol{\epsilon}}[\epsilon_i] = 0$, we can obtain that when m is an odd number, $\mathbb{E}_{\boldsymbol{\epsilon}}[\tilde{\epsilon}_i^m] = 0$. Then,

$$\mathbb{E}_{\boldsymbol{\epsilon}}[(1 + \tilde{\epsilon}_i)^{2\kappa_i}] = 1 + \sum_{m=1}^{\kappa_i} \binom{2\kappa_i}{2m} \mathbb{E}_{\boldsymbol{\epsilon}}[\tilde{\epsilon}_i^{2m}]\tag{21}$$

Furthermore, since different dimensions of the perturbation are independent to each other, the **second-order moment** of $\hat{\pi}(\boldsymbol{\kappa}|\mathbf{x} + \boldsymbol{\epsilon})$ is given as

$$\begin{aligned}\mathbb{E}_{\boldsymbol{\epsilon}}(\hat{\pi}^2(\boldsymbol{\kappa}|\mathbf{x} + \boldsymbol{\epsilon})) &= \mathbb{E}_{\boldsymbol{\epsilon}}[\prod_{i \in S} (1 + \tilde{\epsilon}_i)^{2\kappa_i}] = \prod_{i \in S} \mathbb{E}_{\boldsymbol{\epsilon}}[(1 + \tilde{\epsilon}_i)^{2\kappa_i}] \\ &= \prod_{i \in S} \left(1 + \sum_{m=1}^{\kappa_i} \binom{2\kappa_i}{2m} \cdot \mathbb{E}_{\boldsymbol{\epsilon}}[\tilde{\epsilon}_i^{2m}] \right) = \prod_{i \in S} \left(1 + \sum_{m=1}^{\kappa_i} \binom{2\kappa_i}{2m} \cdot \frac{1}{\tau^{2m}} \mathbb{E}_{\boldsymbol{\epsilon}}[\epsilon_i^{2m}] \right)\end{aligned}\tag{22}$$

Let us use $V_{2m}(\epsilon_i) = \mathbb{E}(\epsilon_i^{2m})$ to denote the $2m$ -order moment of the variable ϵ_i , and use $c_m = \binom{2\kappa_i}{2m} \cdot \frac{1}{\tau^{2m}}$ to denote its coefficient. Then, the conclusion holds. \square